CrystEngComm

PAPER

View Article Online
View Journal | View Issue



Cite this: *CrystEngComm*, 2025, **27**, 4508

# Ladder-type 1D coordination polymer of Dy(III): synthesis and investigation of magnetic behaviour†

Naushad Ahmed, *[a] Rizwan Nabi,[b] Xiaoguang Zhang [b] and Donald J. Darensbourg *[a]

Received 12th May 2025,
Accepted 5th June 2025

DOI: 10.1039/d5ce00491h

rsc.li/crystengcomm

Herein, we report the construction of a H-bonded ladder-type Dy(III) based 1D coordination polymer **1-Dy$_{poly}$** using a 2,6-diacetylpyridine bis-salicyl hydrazone ($H_4L$) ligand system under thermal condition. The X-ray diffraction studies on the reported coordination polymer revealed that it crystallizes in a monoclinic system having the $P2_1/c$ space group. The static and dynamic magnetic behavior of **1-Dy$_{poly}$** was investigated using combined experimental and theoretical tools. The zero-field out-of-phase signals for **1-Dy$_{poly}$** were observed, but with fast under-barrier magnetic relaxation processes. CASSCF-based *ab initio* and BS-DFT calculations were used to rationalize our experimental findings.

## Introduction

In the construction of 1D, 2D coordination polymers (CPs), including metal–organic frameworks, MOFs architecture, the ligands' design plays a vital role in polymeric structure propagation and defining the geometry around the metal ions for various studies.[1–6] There are several examples of multidentate multi-arm ligand systems used for the construction of transition and lanthanide-based CPs and MOFs.[7–9] The crystal field imposed by ligating atoms around the metal ions is reported to governs the spin Hamiltonian SH parameters, which in turn governs the magnetic behaviour of d- and f-block metal ions.[10–13] The fine-tuning in the crystal field around d- and f-block metal ions under different ligand architectures can affect their magnetic and photophysical properties.[14–19] The last few decades have witnessed probing the magnetic properties of lanthanide and transition metal discrete complexes and coordination polymers at the molecular level as single-molecule magnets SMMs that have the feature of slow magnetic relaxations.[20–22] The research area of SMMs has garnered significant attention due to their proposed technological applications in high-density storage devices, molecular spintronics, and quantum computations.[23,24] Due to the unquenched orbital angular momentum and strong spin–orbit coupling, lanthanides exhibit large magnetic anisotropy and are widely used in SMM construction.[25–29] Among the several symmetries, $D_{5h}$ (for pentagonal bipyramidal geometry)[30,31] and $D_{6h}$ (for hexagonal bipyramidal geometry)[32–34] are more popular as in these geometries Dy(III) ions stabilize oblate ground state $m_J$ = 15/2, and have been reported to show high-performance SMMs with an energy barrier up to ~1600 K that are next to metallocene Dy(III) complexes[35,36] having $D_{5d}$ symmetry and an energy barrier up to ~2200 K. The hydrazone ligands derived from Schiff base condensation of 2,6-diacetylpyridine (or 2,6-diformylpyridine) and hydrazide or phenyl-substituted hydrazides are widely explored in constructing the f-block as well as d-block metal coordination complexes. This is due to their ability to provide an equatorial rigid pentagonal plane through $N_3O_2$ donor atoms around metal ions.[37–39] Interestingly, the presence of phenolic –OH on the phenyl ring of 2,6-diacetylpyridine bis-salicylhydrazone ligands opens further coordination opportunities and assembles clusters of multinuclear lanthanide(III) and 3d-lanthanide(III) complexes, including CPs (Fig. 1).[40–44] Several coordination polymers have been reported to date with various applications such as luminescence,[45] proton conduction,[2] gas sorption,[46] and magnetism.[47–49] Since lanthanide metal ions exhibit high coordination numbers and are flexible to variable geometries, the construction of 1D, 2D, and MOFs coordination polymers is challenging to rational design and synthesis. Not only a synthetic challenge, but these polymeric materials also face the challenge to show the expected magnetic property, such as slow magnetic relaxations. Recently, we and others have reported that the intra- and intermolecular dipolar magnetic

[a] *Department of Chemistry, Texas A&M University, College Station, TX 77843, USA. E-mail: naushad.ahmed@tamu.edu, djdarens@chem.tamu.edu*
[b] *Department of Physics, Center for Molecular Magnetic Quantum Materials and Quantum Theory Project, University of Florida, Gainesville, Florida 32611, USA. E-mail: xgz@ufl.edu*

† Electronic supplementary information (ESI) available: Supporting single crystal data, bond parameters, and magnetic data are provided in ESI. CCDC 2433773. For ESI and crystallographic data in CIF or other electronic format see DOI: https://doi.org/10.1039/d5ce00491h

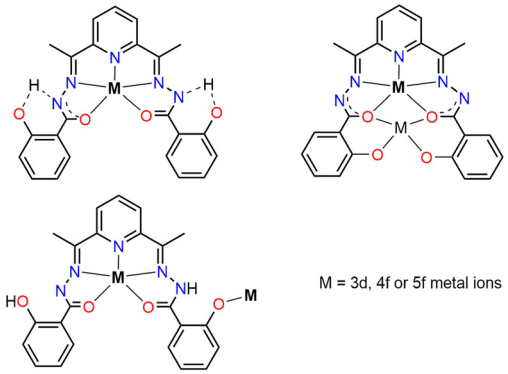


Fig. 1 Coordination modes of 2,6-bis(1-salicyloylhydrazonoethyl)-pyridine ($H_4L$) ligand.

interactions through hydrogen bonding and short contacts may trigger the under-barrier magnetic relaxations such as QTM, and Raman, which may hamper the SMM behaviour.[7,50] This is not surprising in the cases of coordination polymers CPs having extensive hydrogen bonding, π–π, and CH–π stacking interactions that provide structural stability and, on the other hand, may also promote dipolar magnetic interactions, which can suppress their SMM properties.

In this work, we report the construction of a 1D ladder-type coordination polymer of Dy(III) utilizing the phenolic –OH of 2,6-bis(1-salicyloylhydrazonoethyl)-pyridine ($\mathbf{H_4L}$) ligand under thermal conditions. Our several efforts to synthesize Y(III) and Gd(III) coordination polymers under similar conditions as for $\mathbf{1\text{-}Dy_{poly}}$ were not successful. We have investigated the static and dynamic magnetic properties of the reported CPs using experimental and theoretical tools.

## Results and discussion

The reaction of 2,6-diacetylpyridine bis-salicyl hydrazone $\mathbf{H_4L}$ ligand having $N_3O_2$ equatorial donor atoms with hydrated Dy(III) chloride salts in ethanol has led to the isolation of a 1D coordination polymer chain $\mathbf{1\text{-}Dy_{poly}}$ upon heating the solid residue to ~120 °C temperature and dissolving it in hot ethanol solvent (Scheme 1). The dissolution of solid residue directly (as obtained from the reaction) in ethanol solvent produces the $[\mathbf{H_2L}Dy(Cl)_2]Et_3NH$ complex, having Dy(III) in pentagonal bipyramidal geometry, which has been reported elsewhere.[37]

The formation of $\mathbf{1\text{-}Dy_{poly}}$ is proposed to occur *via* tautomerism at higher temperatures; that is, a proton from one of the phenolic –OH permanently shifts to a neighbour deprotonated nitrogen, making the phenolate oxygen available to coordinate, which acts as a linker in this $\mathbf{1\text{-}Dy_{poly}}$. Simultaneously, removing one of the axial $Cl^-$ from other molecules invites phenolate and ethanol ligands to coordinate with Dy(III) from the same side. In this way, the 1D structure of $\mathbf{1\text{-}Dy_{poly}}$ propagates using the phenolate ligating oxygen atoms (Scheme 2).

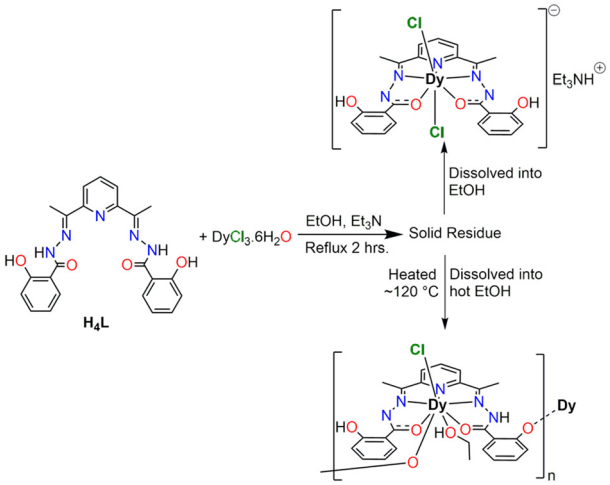


Scheme 1 Synthetic scheme followed to isolate $\mathbf{1\text{-}Dy_{poly}}$.

X-ray diffraction studies revealed that $\mathbf{1\text{-}Dy_{poly}}$ crystallized in a monoclinic crystal system having the $P2_1/c$ space group. From the crystal structure analysis and elucidation, it is found that the asymmetric unit (ASU) of $\mathbf{1\text{-}Dy_{poly}}$ consists of one doubly deprotonated $H_2L^{2-}$ ligand, which uses its $N_3O_2$ donor atoms to create a distorted pentagonal plane around the Dy(III) metal ion from the equatorial positions. Ethanol solvent was coordinated to one of the axial sites of the Dy(III) ion. One of the phenolic oxygens (O1, O1#) present in the ligand was found to be deprotonated and coordinated with the neighbouring Dy(III) metal ion from the same axial side where ethanol is present. This deprotonated phenolic oxygen is responsible for the 1D growth of the ladder-type coordination polymer chain in $\mathbf{1\text{-}Dy_{poly}}$ (see Fig. 2).

The $Cl^-$ ligand occupies the other axial position. The Dy(III) ion is surrounded by eight coordinating atoms with an $N_3O_5$ environment in $\mathbf{1\text{-}Dy_{poly}}$. The continuous shape measurement (CShM)[51] analysis confirms that the distorted triangular dodecahedron geometry (CShM = 4.724) has $D_{2d}$ symmetry around each Dy(III) ion in the chain.

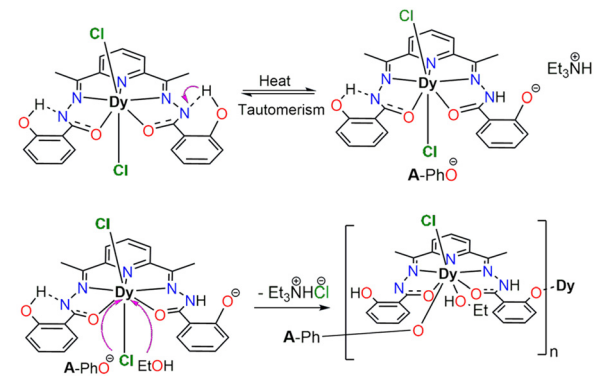


Scheme 2 Proposed mechanism for the formation of $\mathbf{1\text{-}Dy_{poly}}$.

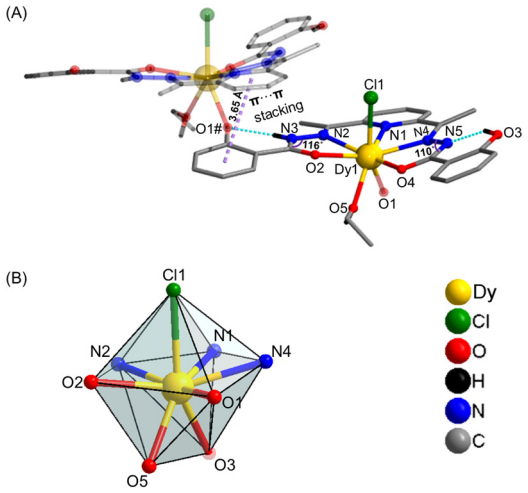


Fig. 2 A) Molecular structure of coordination polymer **1-Dy$_{poly}$**. The part of the molecule present in the asymmetric unit (ASU) is labelled, while the grown structure is shown in translucent. B) Polyhedral view around Dy(III) ion.

## Crystal structure description

The crystal structure analysis of **1-Dy$_{poly}$** confirms the bond distance of 2.524 Å for Dy–N1 (N1 belongs to pyridine) and the bond distances of 2.543 Å and 2.456 Å, respectively, for Dy–N3 and Dy–N4 (N3 and N4 belong to the hydrazides unit). The shorter bond for Dy–N4 indicates that N4 is deprotonated while N3 is not. Furthermore, the equatorial Dy–O2 and Dy–O4 bond distances are 2.273 Å and 2.381 Å, respectively, and show a shorter distance for the deprotonated side of the hydrazone ligand. Along with the bond distances, we also observed a significant difference in the bond angles: ∠N2–N3–C = 115.7°, while ∠N4–N5–C = 110.5°. The bond angle around 111° indicates the absence of H on nitrogen N5.[52]

The axial Dy–Cl and Dy–O1 (O1 from phenolic OH) bond distances were 2.695 Å and 2.306 Å, respectively, while the axial Dy–O5 (O5 from ethanol) bond distance was 2.393 Å.

Primarily the phenolate oxygen donor atoms of the hydrazone ligand play a vital role in propagating the 1D structure in **1-Dy$_{poly}$**, while the π-electron clouds of the pyridine and benzene rings of the neighboring unit further support the structure by π–π stacking interactions within the range of 3.65 Å distance (Fig. 2). The intrachain Dy···Dy distance was found to be 7.475 Å. The packing structure of **1-Dy$_{poly}$** shows the shortest interchain Dy···Dy distance of 10.37 Å, while the interchain distance grown through the hydrogen bonding network (Fig. S2 in ESI†) shows the shortest Dy···Dy distance of 7.546 Å. The shorter interchain Dy···Dy is due to the extensive interchain hydrogen bonding through the axially coordinated ethanol and $Cl^-$ ligands (Fig. 3 and S2 in ESI†).

## Magnetic properties

Direct current magnetic susceptibility measurements were performed on the polycrystalline powder sample of **1-Dy$_{poly}$** in the temperature range of 2–300 K under 1 kOe magnetic field (Fig. 4). The collected data was processed considering the dinuclear molecule having two Dy(III) ions and two full hydrazone ligands along with coordinated $Cl^-$ and ethanol ligands. The observed room temperature $\chi_M T$ value of 27.68 $cm^{-1}$ K $mol^{-1}$ for **1-Dy$_{poly}$** was found to be slightly lower but in close agreement with the theoretical value of 28.34 $cm^{-1}$ K $mol^{-1}$ for two uncoupled $Dy^{III}$ ($S$ = 5/2, $g$ = 4/3, $^6H_{15/2}$). Upon decreasing the temperature, a gradual decrease in the $\chi_M T$ value was observed up to 20 K and below this

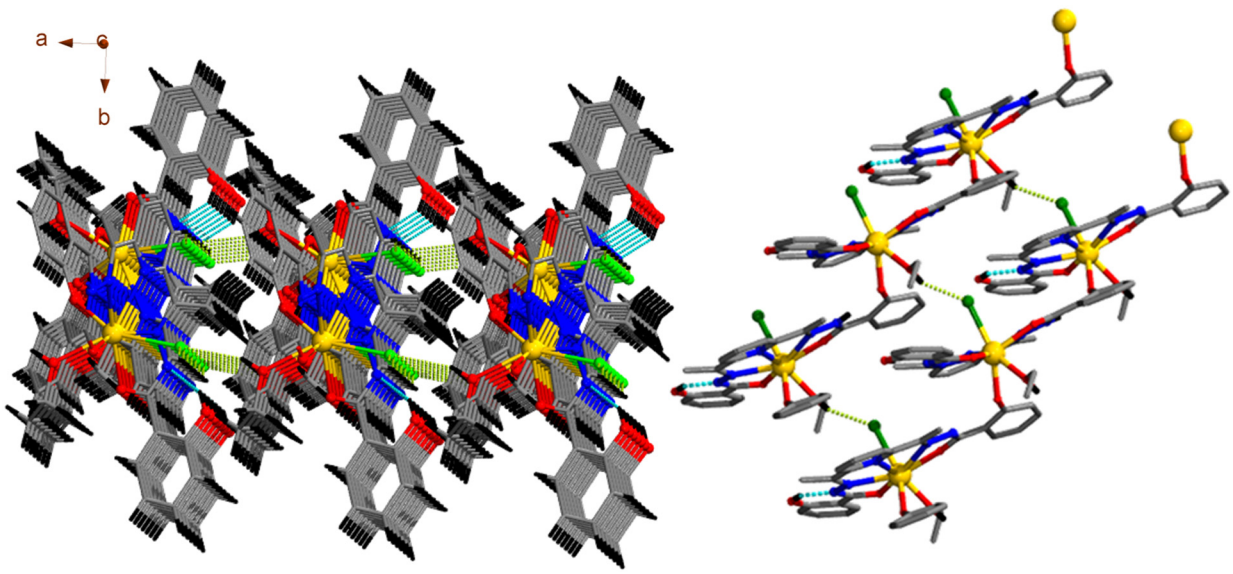


Fig. 3 Intra (sky blue dotted bonds) and intermolecular (light green dotted bonds) hydrogen bonding network in **1-Dy$_{poly}$**.

 

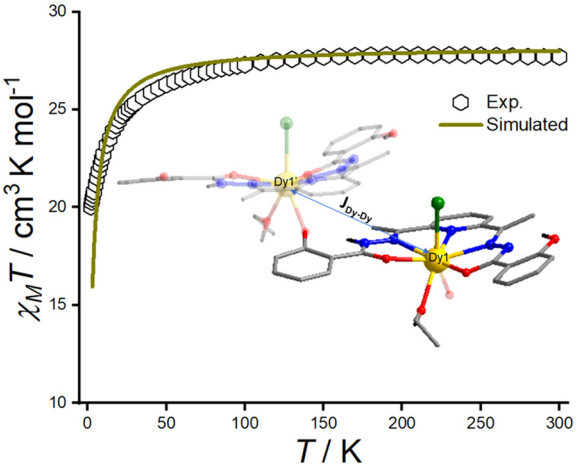


Fig. 4 DC magnetic susceptibility under 1 kOe field. The green solid curve represents the simulated data for **1-Dy$_{poly}$**.

temperature, a sudden drop in the $\chi_M T$ value was observed and reached the minimum value of 20 cm$^{-1}$ K mol$^{-1}$ at 2 K. This can be attributed to the depopulation of the excited Stark or $\pm m_J$ levels of Dy$^{III}$ ion, while the low temperature $\chi_M T$ profile of **1-Dy$_{poly}$** is due to the intra- and interchain antiferromagnetic interactions. As stated in the crystal structure description section, the shortest Dy⋯Dy inter- and intrachain distances were found to be ~7 Å, suggesting dipolar magnetic interactions are highly possible in **1-Dy$_{poly}$**. Field-dependent magnetization data were collected at 2–8 K temperature and magnetic field from zero to 70 kOe (Fig. S6 in ESI†).

To estimate the inter- and intrachain magnetic exchange between Dy(III) ions, we have utilized the computed crystal field axial parameters $B_k^q$ = −1.33 (where $k$ = 2 and $q$ = 0) and $g_{Dy}$ value of 1.33 to simulate the magnetic susceptibility data using the PHI program[53] (Fig. 4). In this case, since the overall exchange energy for intra- or interchain Dy–Dy magnetic interactions can be represented as $J$ or $zJ$, during simulation, we considered the $zJ$, which reproduced the experimental data well with $zJ$ = −0.02 cm$^{-1}$.

Dynamic magnetic susceptibility measurements were carried out under zero and applied field in the frequency range of 1–10$^3$ Hz and temperature range 1.8 to 4 K. The field-dependent ac magnetic susceptibility measurements at 1.8 K and applied field up to 3 kOe indicate no clear maxima for the out-of-phase susceptibility $\chi_M''$ signals in the instrumental frequency range, while the zero field broad $\chi_M''$ signals appeared at higher frequency above 10$^2$ Hz, which suggest that **1-Dy$_{poly}$** behaves as zero-field single-molecule magnets but with faster under barrier magnetic relaxations such as quantum tunnelling (QTM) and Raman processes. The application of a dc magnetic field is reported to suppress the QTM processes between the degenerate $\pm m_J$ states and supports arriving and or resolving the $\chi_M''$ signals maximum.[54] On the contrary, we observed the intensity of the applied field $\chi_M''$ signals decrease with increasing field strength; this seems to be a direct magnetic relaxation process that becomes active and faster, and for this reason, **1-Dy$_{poly}$** fails to show improved SMM behaviour.

Despite the broad $\chi_M''$ signals observed at zero field, we were interested in understanding the slow-magnetic relaxation behavior of **1-Dy$_{poly}$** and the presence of under-barrier magnetic relaxation at higher temperatures. To this end, we collected detailed ac data at zero-field in the temperature range of 1.8 K to 4 K. We observed $\chi_M''$ signals maximum centred at 210 Hz, which were not significantly shifted with temperature (Fig. 5). We constructed Cole–Cole plots $\{\chi_M'' = f(\chi_M')\}$ but were unable to fit the curves to extract relaxation times ($\tau$) and relaxation distribution parameter ($\alpha$).

However, the *ab initio* CASSCF/SO-RASSI/SINGLE_ANISO calculations performed on the single crystal X-ray structure of **1-Dy$_{poly}$** indicate the axial nature of Dy(III) ion with ground state $g_{zz}$ = 19.47 and the first excited state Kramers' doublet KD2 located at 115 cm$^{-1}$ from the ground state KD1 (see the computational studies). These observations suggest that the extensive hydrogen bonding (inter- and intrachain) may enforce dipolar interactions and suppress the SMM properties in **1-Dy$_{poly}$** by triggering the underbarrier magnetic relaxation processes.

## Computational studies

The CASSCF-based *ab initio* calculations were performed on the X-ray structure of **1-Dy$_{poly}$** using OpenMolcas v24.02 software.[55] Since the asymmetric unit of **1-Dy$_{poly}$** consists of one metal ion, we have considered all the ligands present in

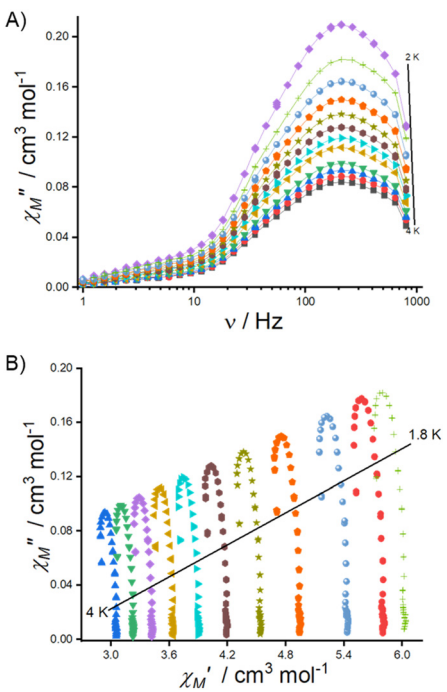


Fig. 5 Zero-field out-of-phase magnetic susceptibility (top A) and Cole–Cole plot (bottom B) for **1-Dy$_{poly}$**.

the ASU when performing our calculations. We also performed DFT calculations to understand the magnetic exchange between intrachain as well as interchain Dy(III) ions. The detailed *ab initio* and DFT calculation methods were discussed in the Experimental section. The CASSCF computed spin-free and spin–orbit states are provided in Tables S3 and S4 in the ESI.† The computed *g*-tensors associated with the ground state Kramers doublet KD1 (arising from $^6H_{15/2}$) of Dy(III) ion ($g_{xx}$ = 0.104, $g_{yy}$ = 0.271, and $g_{zz}$ = 19.470) suggest that **1-Dy$_{poly}$** has a moderately strong axial anisotropic nature. Moreover, as we move further from the ground state, the transversal anisotropy is increased as $g_{xx}$ = 3.052, $g_{yy}$ = 5.669, and $g_{zz}$ = 12.611 at the first excited state (Table 1). The LoProp charge densities on the coordinated atoms are listed in Table S5.† The ground state main magnetization axis ($g_{zz}$) was found perpendicular to $N_3O_2$ equatorial plane around Dy(III) while parallel to the axially coordinated ligands. The ground state $g_{zz}$ axis is oriented along the Dy–Cl (charge density on Cl = −0.87) bond and between the Dy–O5 and Dy–O1 (charge density on O5 = −0.48 and O1 = −0.80) bonds. The $g_{zz}$ axis deviates about 13.63° from the Dy–Cl axis (Fig. 6). Further, computed wave function analysis (Table S6†) confirms the ground state $m_J$ = ±15/2 (KD1) with purity up to ~95% and the transition magnetic moment 6.25 × $10^{-2}$ $\mu_B$ between KD1 indicates magnetization relaxation through a tunnelling process is slow enough to observe zero-field SMM behavior for **1-Dy$_{poly}$**. It should have an *ab initio* energy barrier of ~115 $cm^{-1}$. To shed light on this observation, we also computed crystal parameters using the Hamiltonian $\widehat{H} = \sum \sum_{k=-q}^{q} B_k^q O_k^q$ where the terms $B_k^q$ and $O_k^q$ are the crystal field parameters and Stevens' operator, respectively. The computed crystal field parameters are listed in Table S7 in the ESI.† The axial term $B_2^0$ found to be negative ($B_2^0$ = −1.33) that further suggests easy axis of anisotropy associated Dy(III) ion. Despite the strong axiality associated with Dy(III) ion, the observed experimental dynamic magnetic behavior of **1-Dy$_{poly}$** exhibits faster under-barrier magnetic relaxations, such as QTM and or Raman processes. The presence of extensive H-bonding is expected to trigger these under-barrier magnetic relaxation processes by promoting dipolar magnetic interactions.

Table 1 Magnetic anisotropy data along with the calculated energy barrier to the magnetization relaxation in **1-Dy$_{poly}$** using CASSCF *ab initio* calculations

| Mult. | $E$ ($cm^{-1}$) | $g_x$ | $g_y$ | $g_z$ |
|---|---|---|---|---|
| 1 | 0.0 | 0.104 | 0.271 | 19.470 |
| 2 | 115.1 | 3.052 | 5.670 | 12.611 |
| 3 | 153.7 | 8.246 | 5.439 | 0.768 |
| 4 | 179.6 | 1.575 | 6.337 | 11.830 |
| 5 | 216.6 | 0.365 | 2.325 | 10.974 |
| 6 | 301.5 | 1.040 | 2.113 | 14.921 |
| 7 | 392.8 | 0.247 | 2.282 | 14.249 |
| 8 | 415.9 | 0.319 | 2.164 | 15.432 |

Further to understand the presence of inter and intrachain magnetic exchange (if any) in **1-Dy$_{poly}$**, we modelled dimeric **Gd$_2$$^{mod-1}$** (intrachain) and **Gd$_2$$^{mod-2}$** (interchain) models respectively by replacing the Dy with Gd from the grown structures and performed BS-DFT calculations using B3LYP[56] density-functional. The computed spin densities on Gd(III) ions for high-spin and broken symmetry are listed in Table S8 in the ESI.† The spin density plots are given in Fig. 7. We have used the $H = -2JS_1S_2$ formalism to calculate the magnetic exchange parameter, leading to the weak antiferromagnetic coupling parameter of $J_{Gd-Gd}$ = −0.0003 $cm^{-1}$ between two Gd ions in **Gd$_2$$^{mod-1}$** while for **Gd$_2$$^{mod-2}$** this is −0.0001 $cm^{-1}$. Upon rescaling the $J$ values to the spin of Dy(III) ($S$ = 5/2) we obtained $J_{Dy-Dy}$ = −0.0002 $cm^{-1}$ and −0.00007 $cm^{-1}$ for the intra and interchain Dy–Dy magnetic exchange interactions respectively. The magnetic exchange is found to be very weak but it seems influence the dynamic properties strongly.

# Experimental

Ligand **H$_4$L** was synthesized following the synthetic procedure[57] and used to isolate the coordination polymer **1-Dy$_{poly}$**. A Bruker D8 Venture APEX-II CCD diffractometer was employed for single-crystal X-ray diffraction data collection. SHELXTL and Olex2.4 software were used for X-ray data analysis and structural solutions. The Quantum Design MPMS3 SQUID magnetometer was used for magnetic measurements. A straw was utilized as the sample holder, and the crushed powder sample was tightly wrapped in Teflon tape and inserted into the straw.

### Synthesis of 1-Dy$_{poly}$

In a round-bottom flask, 50 mg of **H$_4$L** ligand (0.1159 mmol) was suspended in 50 mL of ethanol. At 60 °C, the dropwise addition of an ethanolic solution of $DyCl_3·6H_2O$ (43.68 mg, 0.1159 mmol) turns the reaction mixture a transparent yellow color. After 1 hour of stirring at the same temperature, the reaction mixture was brought to room temperature, and two equivalents of triethylamine (0.032 mL, 0.2317 mmol) were added. The slightly turbid reaction mixture was further stirred at 60 °C for two hours, and the solvent was evaporated to dryness. The yellow solid residue was heated up to 120 °C for 2–3 hours. During this period of heating, the solid residue turned dark yellow, which was dissolved in 2 mL of hot ethanol solvent, and hexane was diffused into this solution. The X-ray quality yellow-colored single crystals were grown within a week in good yield, 35 mg (45% based on **H$_4$L** ligand). The C=N and C=O bonds characteristic bands appeared at $\nu_{(C=N)}$ = 1612 $cm^{-1}$ and $\nu_{(C=O)}$ = 1593 $cm^{-1}$ respectively in FT-IR spectrum (Fig. S3†). Powder X-ray diffraction data collected in a 2$\theta$ range of 5 to 40° and plotted over the pattern obtained from single-crystal X-ray diffraction (Fig. S4†). The thermogravimetric analysis revealed that **1-Dy$_{poly}$** is thermally stable up to 300 °C (Fig. S5†) with almost no weight loss.

 

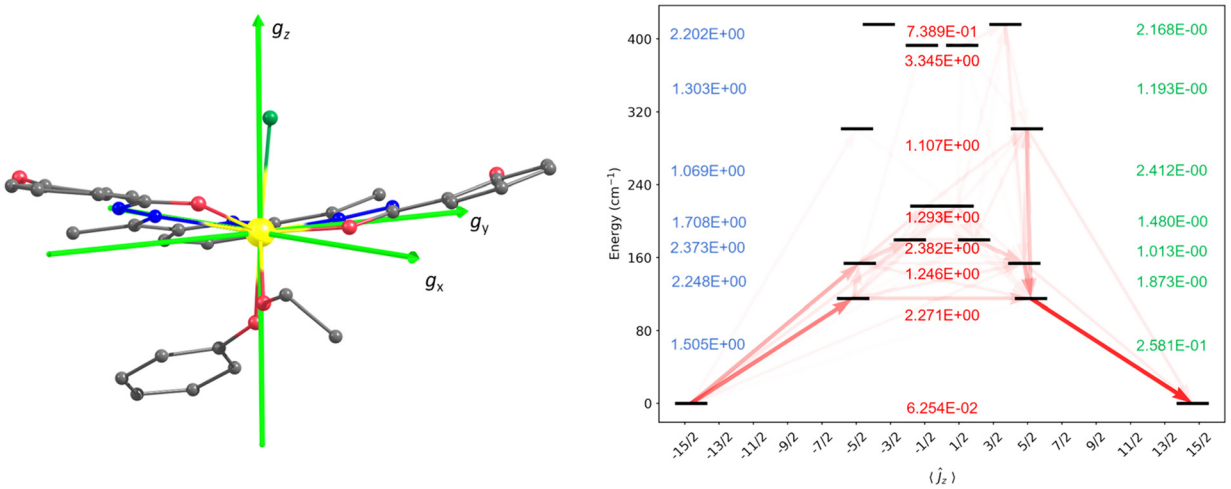


**Fig. 6** The direction of the computed ground state main magnetization axis $g_{zz}$ (left) and the plausible magnetic relaxation mechanism (right). Dark red arrows indicate a larger absolute value of the transition magnetic moment matrix elements between the respective states. The relaxation mechanism omits transitions involving higher-energy states that are not involved in the relaxation mechanism.

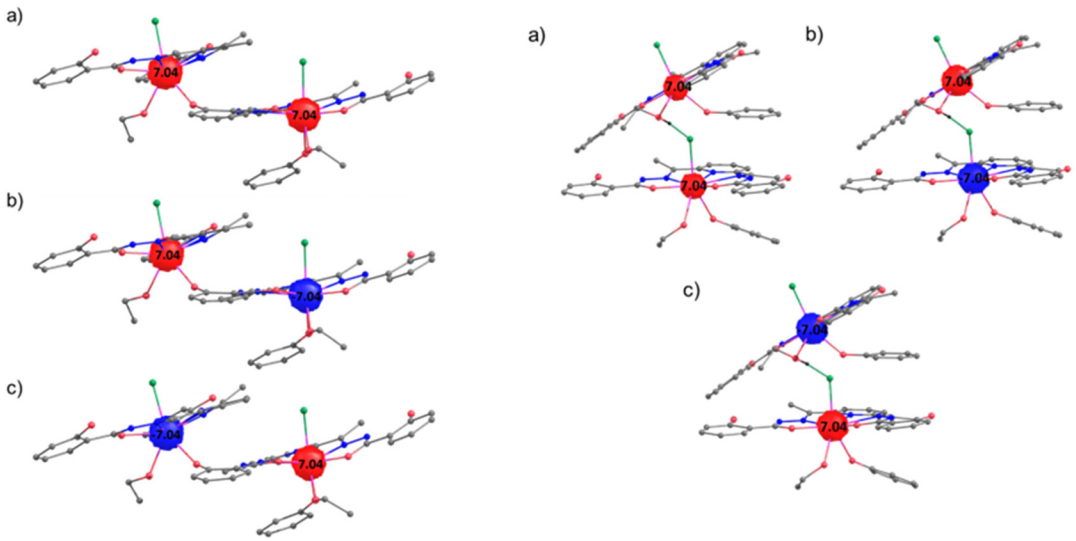


**Fig. 7** Spin density plots for $\mathbf{Gd_2}^{\mathbf{mod\text{-}1}}$ (left) and $\mathbf{Gd_2}^{\mathbf{mod\text{-}2}}$ (right). a) High-spin state, b) broken symmetry 1 (BS1) where Gd1 is spin down, and c) broken symmetry 2 (BS2) where Gd2 is spin down. Color code: red corresponds to positive spin density, and blue corresponds to the spin-down state.

## Computational details

***Ab initio*.** All calculations were done on the crystal structure obtained from the experiments without further optimization of geometry. All the first-principle *ab initio* calculations CASSCF/RASSI-SO/SINGLE_ANISO were performed using the OpenMolcas v24.02 program package. We have employed the Douglas–Kroll–Hess (DKH) Hamiltonian, which considers the relativistic effects corresponding to metal ions.[58] In our calculation, we used ANO-RCC (atomic natural orbital-relativistically core correlated) type of basis sets for all the atoms in **1-Dy$_{poly}$**. ANO-RCC-VTZP basis set was used for Dy(III) ion, ANO-RCC-VDZP for the rest of the atoms such as C, H N, and O. While considering the active space, we used nine electrons in seven 4f orbitals of Dy(III) for the complete active space self-consistent field (CASSCF) calculations. During spin-state calculations, 21 sextet, 224 doublet, and 490 doublet roots were calculated, while only the twenty-one spin-free states were mixed to get the energies of spin-free and spin–orbit states in the RASSI-SO module. To compute g-tensors, dc magnetic properties, and plausible magnetic relaxation pathways, the SINGLE_ANISO module was used.

**DFT.** For the determination of the exchange coupling in $\mathbf{Gd_2}^{\mathbf{mod\text{-}1}}$ and $\mathbf{Gd_2}^{\mathbf{mod\text{-}2}}$, we employed broken-symmetry DFT calculations. The BS-DFT calculations were performed with the Gaussian16 package. The B3LYP density-functional was used in conjunction with the 6-31G* basis set for Cl, O, N, C,

and H atoms,[59] the 46 core electron Cundari Stevens Double Zeta ECP and the corresponding valence basis set were employed for Gd.[60] Calculations were performed for the high-spin and broken-symmetry solutions, leading to the exchange coupling values obtained using the Noodleman method.[61] In all DFT calculations, the ultrafine grid (gd3) was taken into consideration.

## Conclusions

In summary, we have utilized the phenolic –OH of 2,6-diacetylpyridine bis-salicyl hydrazone (**$H_4L$**) ligand system to construct a 1D ladder-type Dy(III) coordination polymer. The proton of the phenolic –OH shifted to one of the deprotonated N atoms at around 120 °C and facilitated the 1D structure propagation through a phenolate linker. Dynamic magnetic measurement of reported polymer indicates zero-field SMM but has faster QTM and or Raman magnetic relaxation processes. CASSCF-based *ab initio* calculation revealed that the Dy(III) ion experiences a moderate axial nature, but due to extensive inter- and intrachain hydrogen bonding, particularly through the axially coordinated ethanol and $Cl^-$ ligands, triggers the under-barrier magnetic relaxation and suppresses SMM behavior.

## Data availability

We have provided the data in the ESI.† X-ray data for the crystal structure can be accessed through the CCDC 2433773.

## Conflicts of interest

There are no conflicts of interest to declare.

## Acknowledgements

DJD gratefully acknowledges the Robert A. Welch Foundations (A-0923) for financial support. NA thanks the Department of Chemistry, Texas A&M University, for accessing the research facilities. RN and Zhang thank UF HiPerGator for the computational facilities. This research was supported as part of the Center for Molecular Magnetic Quantum Materials, an Energy Frontier Research Center funded by the U.S. Department of Energy, Office of Science, Basic Energy Sciences under Award No. DE-SC0019330.

## References

1 C.-L. Chen, C. Wang, X.-Y. Zheng, R. Zhang, Y. Xu, G.-L. Zhuang, L.-S. Long, L.-S. Zheng, X.-J. Kong and Y. Cao, *J. Am. Chem. Soc.*, 2023, **145**, 16983–16987.
2 S. C. Pal, D. Mukherjee, Y. Oruganti, B. G. Lee, D.-W. Lim, B. Pramanik, A. K. Manna and M. C. Das, *J. Am. Chem. Soc.*, 2024, **146**, 14546–14557.
3 M.-X. Hong, Z.-H. Wu, C. Chen, L. Cao, H. Tian and X.-Y. Zheng, *Polyhedron*, 2024, **251**, 116847.
4 Z.-P. Zhao, K. Zheng, H.-R. Li, C.-H. Zeng, S. Zhong, S. W. Ng, Y. Zheng and Y. Chen, *Inorg. Chim. Acta*, 2018, **482**, 340–346.
5 F. Li, L. Xu, B. Bi, X. Liu and L. Fan, *CrystEngComm*, 2008, **10**, 693–698.
6 G. Mínguez Espallargas and E. Coronado, *Chem. Soc. Rev.*, 2018, **47**, 533–557.
7 G. A. Ramakant, N. Ahmed, I. Tarannum, S. Mehta, M. Nandeshwar, A. Mondal, S. K. Singh and G. Prabusankar, *Cryst. Growth Des.*, 2022, **22**, 6046–6055.
8 C. Theppitak, S. Jiajaroen, N. Chongboriboon, S. Chanthee, F. Kielar, W. Dungkaew, M. Sukwattanasinitt and K. Chainok, *Molecules*, 2021, **26**, 4428.
9 M. Yadav, A. Bhunia, S. K. Jana and P. W. Roesky, *Inorg. Chem.*, 2016, **55**, 2701–2708.
10 A. K. Bar, C. Pichon and J.-P. Sutter, *Coord. Chem. Rev.*, 2016, **308**, 346–380.
11 G. Charron, F. Bellot, F. Cisnetti, G. Pelosi, J.-N. Rebilly, E. Rivière, A.-L. Barra, T. Mallah and C. Policar, *Chem. – Eur. J.*, 2007, **13**, 2774–2782.
12 T. Goswami and A. Misra, *J. Phys. Chem. A.*, 2012, **116**, 5207–5215.
13 E. M. Manohar, T. Guizouarn, N. Ahmed, R. Herchel, F. Pointillart, S. Das and A. Dey, *Appl. Organomet. Chem.*, 2024, **38**, e7441.
14 J. D. Rinehart and J. R. Long, *Chem. Sci.*, 2011, **2**, 2078–2085.
15 C. Wegeberg, D. Häussinger, S. Kupfer and O. S. Wenger, *J. Am. Chem. Soc.*, 2024, **146**, 4605–4619.
16 M. Kong, X. Feng, J. Wang, Y.-Q. Zhang and Y. Song, *Dalton Trans.*, 2021, **50**, 568–577.
17 A. Raza and M. Perfetti, *Coord. Chem. Rev.*, 2023, **490**, 215213.
18 H. Wu, M. Li, B. Yin, Z. Xia, H. Ke, Q. Wei, G. Xie, S. Chen and S. Gao, *Dalton Trans.*, 2019, **48**, 16384–16394.
19 S. Roy, P. Shukla, N. Ahmed, M.-H. Du, I. Tarannum, X.-J. Kong, T. Gupta, S. K. Singh and S. Das, *Dalton Trans.*, 2022, **51**, 18187–18202.
20 A. Zabala-Lekuona, J. M. Seco and E. Colacio, *Coord. Chem. Rev.*, 2021, **441**, 213984.
21 A. B. Ruiz-Muelle, A. García-García, A. A. García-Valdivia, I. Oyarzabal, J. Cepeda, J. M. Seco, E. Colacio, A. Rodríguez-Diéguez and I. Fernández, *Dalton Trans.*, 2018, **47**, 12783–12794.
22 L. Rigamonti, M. Vaccari, F. Roncaglia, C. Baschieri and A. Forni, *Magnetochemistry*, 2018, **4**(4), 43.
23 J. J. Baldoví, L. E. Rosaleny, V. Ramachandran, J. Christian, N. S. Dalal, J. M. Clemente-Juan, P. Yang, U. Kortz, A. Gaita-Ariño and E. Coronado, *Inorg. Chem. Front.*, 2015, **2**, 893–897.
24 J. J. Baldoví, S. Cardona-Serra, J. M. Clemente-Juan, E. Coronado, A. Gaita-Ariño and A. Palii, *Inorg. Chem.*, 2012, **51**, 12565–12574.
25 D. N. Woodruff, R. E. P. Winpenny and R. A. Layfield, *Chem. Rev.*, 2013, **113**, 5110–5148.
26 N. Ahmed and D. J. Darensbourg, *Cryst. Growth Des.*, 2025, **25**, 1992–2001.

 

27 A. Dey, P. Kalita and V. Chandrasekhar, *ACS Omega*, 2018, **3**, 9462–9475.
28 N. Ahmed and K. U. Ansari, *Dalton Trans.*, 2022, **51**, 8766–8776.
29 N. Ahmed and K. Uddin Ansari, *Dalton Trans.*, 2022, **51**, 4122–4134.
30 J. Liu, Y.-C. Chen, J.-L. Liu, V. Vieru, L. Ungur, J.-H. Jia, L. F. Chibotaru, Y. Lan, W. Wernsdorfer, S. Gao, X.-M. Chen and M.-L. Tong, *J. Am. Chem. Soc.*, 2016, **138**, 5441–5450.
31 Y.-C. Chen, J.-L. Liu, L. Ungur, J. Liu, Q.-W. Li, L.-F. Wang, Z.-P. Ni, L. F. Chibotaru, X.-M. Chen and M.-L. Tong, *J. Am. Chem. Soc.*, 2016, **138**, 2829–2837.
32 S. Jia, X. Zhu, B. Yin, Y. Dong, A. Sun and D.-F. Li, *Cryst. Growth Des.*, 2023, **23**, 6967–6973.
33 J. Li, S. Gómez-Coca, B. S. Dolinar, L. Yang, F. Yu, M. Kong, Y.-Q. Zhang, Y. Song and K. R. Dunbar, *Inorg. Chem.*, 2019, **58**, 2610–2617.
34 A. B. Canaj, S. Dey, E. R. Martí, C. Wilson, G. Rajaraman and M. Murrie, *Angew. Chem., Int. Ed.*, 2019, **58**, 14146–14151.
35 F.-S. Guo, B. M. Day, Y.-C. Chen, M.-L. Tong, A. Mansikkamäki and R. A. Layfield, *Science*, 2018, **362**, 1400–1403.
36 F.-S. Guo, B. M. Day, Y.-C. Chen, M.-L. Tong, A. Mansikkamäki and R. A. Layfield, *Angew. Chem., Int. Ed.*, 2017, **56**, 11445–11449.
37 A. K. Bar, P. Kalita, J.-P. Sutter and V. Chandrasekhar, *Inorg. Chem.*, 2018, **57**, 2398–2401.
38 P. Kalita, N. Ahmed, A. K. Bar, S. Dey, A. Jana, G. Rajaraman, J.-P. Sutter and V. Chandrasekhar, *Inorg. Chem.*, 2020, **59**, 6603–6612.
39 A. K. Bar, N. Gogoi, C. Pichon, V. M. L. D. P. Goli, M. Thlijeni, C. Duhayon, N. Suaud, N. Guihéry, A.-L. Barra, S. Ramasesha and J.-P. Sutter, *Chem. – Eur. J.*, 2017, **23**, 4380–4396.
40 P. Kalita, K. Kumari, P. Kumar, V. Kumar, S. K. Singh, G. Rogez and V. Chandrasekhar, *Dalton Trans.*, 2024, **53**, 10521–10535.
41 H.-Q. Li, G.-L. Wang, Y.-C. Sun, Y.-Q. Zhang and X.-Y. Wang, *Inorg. Chem.*, 2022, **61**, 17537–17549.
42 H.-Q. Li, Y.-C. Sun, L. Shi, F.-L. Chen, F.-X. Shen, Y. Zhao and X.-Y. Wang, *Inorg. Chem.*, 2022, **61**, 2272–2283.
43 V. Singh, L. T. Suresh, J.-P. Sutter and A. K. Bar, *Dalton Trans.*, 2024, **53**, 7436–7449.
44 R. Wang, H. Wang, J. Wang, F. Bai, Y. Ma, L. Li, Q. Wang, B. Zhao and P. Cheng, *CrystEngComm*, 2020, **22**, 2998–3004.
45 P. Chen, Q. Li, S. Grindy and N. Holten-Andersen, *J. Am. Chem. Soc.*, 2015, **137**, 11590–11593.
46 M. Lippi and M. Cametti, *Coord. Chem. Rev.*, 2021, **430**, 213661.
47 T. Grancha, J. Ferrando-Soria, M. Castellano, M. Julve, J. Pasán, D. Armentano and E. Pardo, *Chem. Commun.*, 2014, **50**, 7569–7585.
48 X.-T. Dong, M.-Q. Yu, Y.-B. Peng, G.-X. Zhou, G. Peng and X.-M. Ren, *Dalton Trans.*, 2023, **52**, 12686–12694.
49 C.-M. Liu, D.-Q. Zhang, J.-B. Su, Y.-Q. Zhang and D.-B. Zhu, *Inorg. Chem.*, 2018, **57**, 11077–11086.
50 S. K. Gupta, S. Dey, T. Rajeshkumar, G. Rajaraman and R. Murugavel, *Chem. – Eur. J.*, 2022, **28**, e202103585.
51 M. Pinsky and D. Avnir, *Inorg. Chem.*, 1998, **37**, 5575–5582.
52 J.-P. Sutter, V. Béreau, V. Jubault, K. Bretosh, C. Pichon and C. Duhayon, *Chem. Soc. Rev.*, 2022, **51**, 3280–3313.
53 N. F. Chilton, R. P. Anderson, L. D. Turner, A. Soncini and K. S. Murray, *J. Comput. Chem.*, 2013, **34**, 1164–1175.
54 N. Malinová, J. Juráková, B. Brachňaková, J. D. Midlíková, E. Čižmár, V. T. Santana, R. Herchel, M. Orlita, I. Mohelský, J. Moncol, P. Neugebauer and I. Šalitroš, *Cryst. Growth Des.*, 2023, **23**, 2430–2441.
55 I. F. Galván, M. Vacher, A. Alavi, C. Angeli, F. Aquilante, J. Autschbach, J. J. Bao, S. I. Bokarev, N. A. Bogdanov, R. K. Carlson, L. F. Chibotaru, J. Creutzberg, N. Dattani, M. G. Delcey, S. S. Dong, A. Dreuw, L. Freitag, L. M. Frutos, L. Gagliardi, F. Gendron, A. Giussani, L. González, G. Grell, M. Guo, C. E. Hoyer, M. Johansson, S. Keller, S. Knecht, G. Kovačević, E. Källman, G. Li Manni, M. Lundberg, Y. Ma, S. Mai, J. P. Malhado, P. Å. Malmqvist, P. Marquetand, S. A. Mewes, J. Norell, M. Olivucci, M. Oppel, Q. M. Phung, K. Pierloot, F. Plasser, M. Reiher, A. M. Sand, I. Schapiro, P. Sharma, C. J. Stein, L. K. Sørensen, D. G. Truhlar, M. Ugandi, L. Ungur, A. Valentini, S. Vancoillie, V. Veryazov, O. Weser, T. A. Wesołowski, P.-O. Widmark, S. Wouters, A. Zech, J. P. Zobel and R. Lindh, *J. Chem. Theory Comput.*, 2019, **15**, 5925–5964.
56 A. D. Becke, *J. Chem. Phys.*, 1993, **98**, 5648–5652.
57 C. Pelizzi and G. Pelizzi, *J. Chem. Soc., Dalton Trans.*, 1980, 1970–1973.
58 M. Reiher, *Theor. Chem. Acc.*, 2006, **116**, 241–252.
59 R. Ditchfield, W. J. Hehre and J. A. Pople, *J. Chem. Phys.*, 1971, **54**, 724–728.
60 T. R. Cundari and W. J. Stevens, *J. Chem. Phys.*, 1993, **98**, 5555–5565.
61 L. Noodleman, D. A. Case and A. Aizman, *J. Am. Chem. Soc.*, 1988, **110**, 1001–1005.